Electronic Supporting Information

High Pressure High Temperature Synthesis of Highly Boron Doped Diamond Microparticles and Porous Electrodes for Electrochemical Applications

Georgia F. Wood,[a,b] Carmen E. Zvoriste-Walters,[c] Mark G. Munday,[c] Viacheslav Shkirskiy,[a] Patrick R. Unwin[a] and Julie V. Macpherson[a]*

[a] Department of Chemistry, University of Warwick, Coventry, United Kingdom

[b] Diamond Science and Technology Centre for Doctoral Training, University of Warwick, Coventry, United Kingdom

[c] Element Six, Global Innovation Centre, Didcot, United Kingdom

Table of Contents

ESI 1: Three-electrode droplet electrochemical cell setup

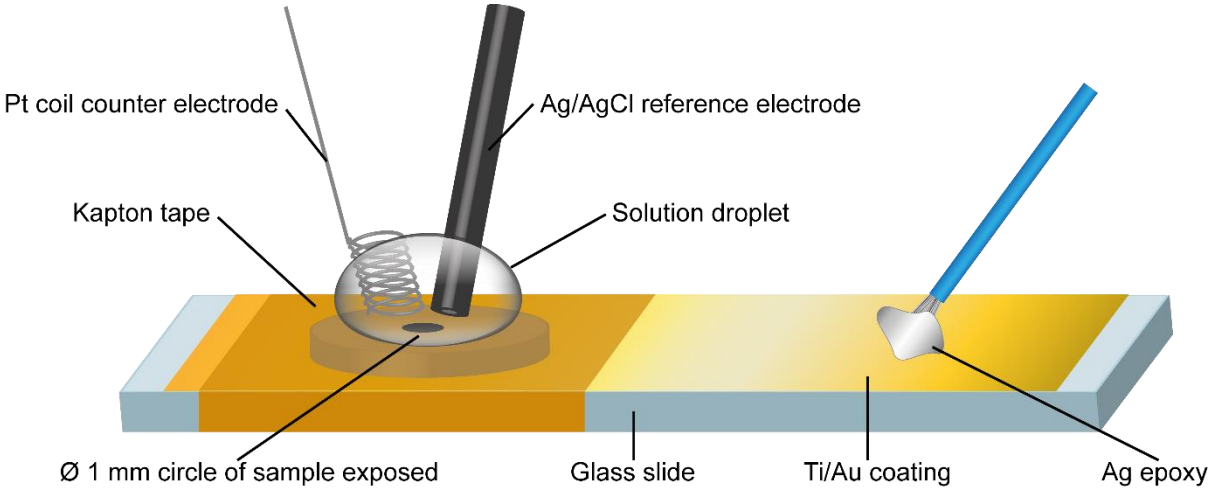

Figure S1. Schematic showing the three-electrode droplet cell set-up for electrochemical characterisation of the HPHT BDD compact electrode.

ESI 2: SECCM experimental setup

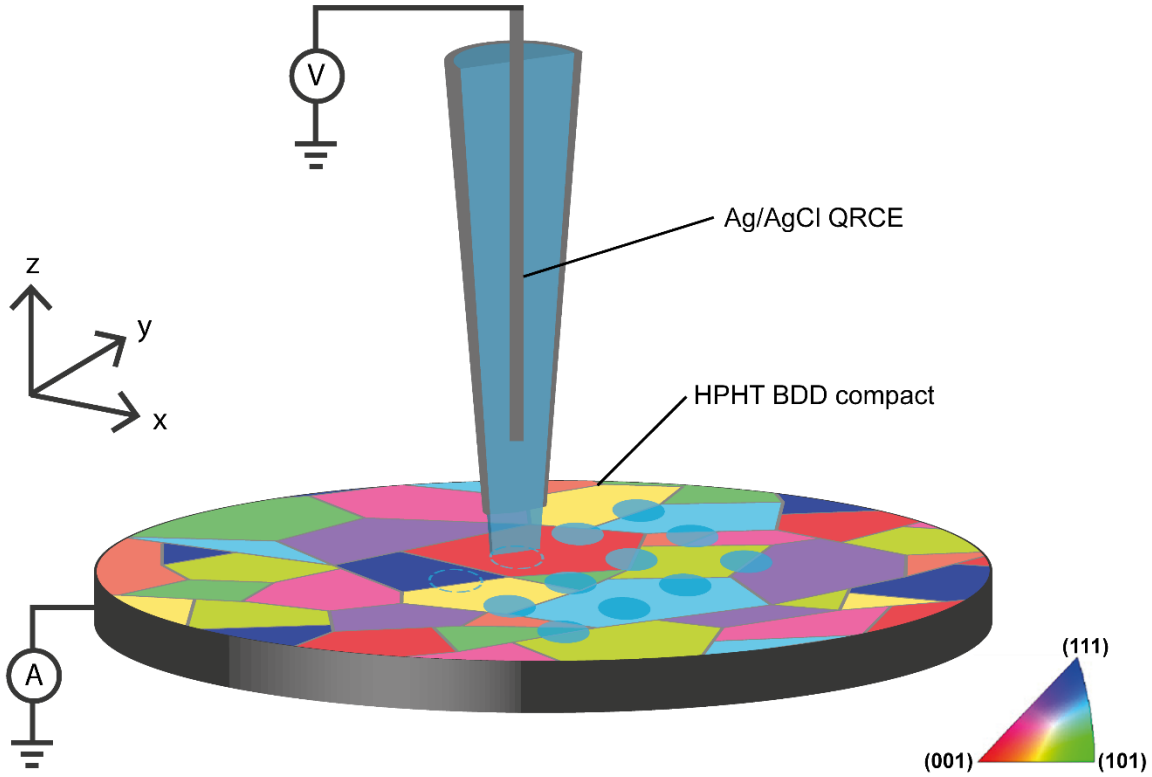

Figure S2. Schematic showing the SECCM experimental set-up used to measure the local electrochemical response of a HPHT BDD compact electrode, grown using 4.8 wt% AlB_2. A scan rate of 10 V s^{-1} was used for the CVs recorded at each pixel location (n = 400, indicated by blue circles). The potential is applied to the Ag/AgCl quasi-reference-counter electrode (QRCE) in the nanopipette, with respect to the compact electrode (grounded) and the current measured at the compact surface (working electrode). The colored surface represents an EBSD map of BDD crystallographic orientation.

ESI 3: The model of bald-point BDD growth

On the {111} diamond face, each carbon atom forms bonds with three neighbouring carbon atoms, leaving a single dangling bond through which the crystal extends during growth. Conversely, on the {100} diamond face, each carbon atom forms bonds with two neighbouring carbon atoms, leaving two dangling bonds through which the crystal extends during growth. In metallic doped BDD, boron atoms substitute ~ 1 in 1000 carbon atoms. As boron only has three valence electrons (as opposed to carbon's four) when a boron atom sits in place of a carbon atom on the {111} face, there is no dangling bond for carbon atoms to bond to (Fig. S3) and so no further growth can occur from this point, leaving bald-points on the {111} surface. However, when a boron atom sits in place of a carbon atom on the {100} face, there is a single dangling bond for carbon atoms to bond to (Fig. S3), and thus crystal growth continues.[1]

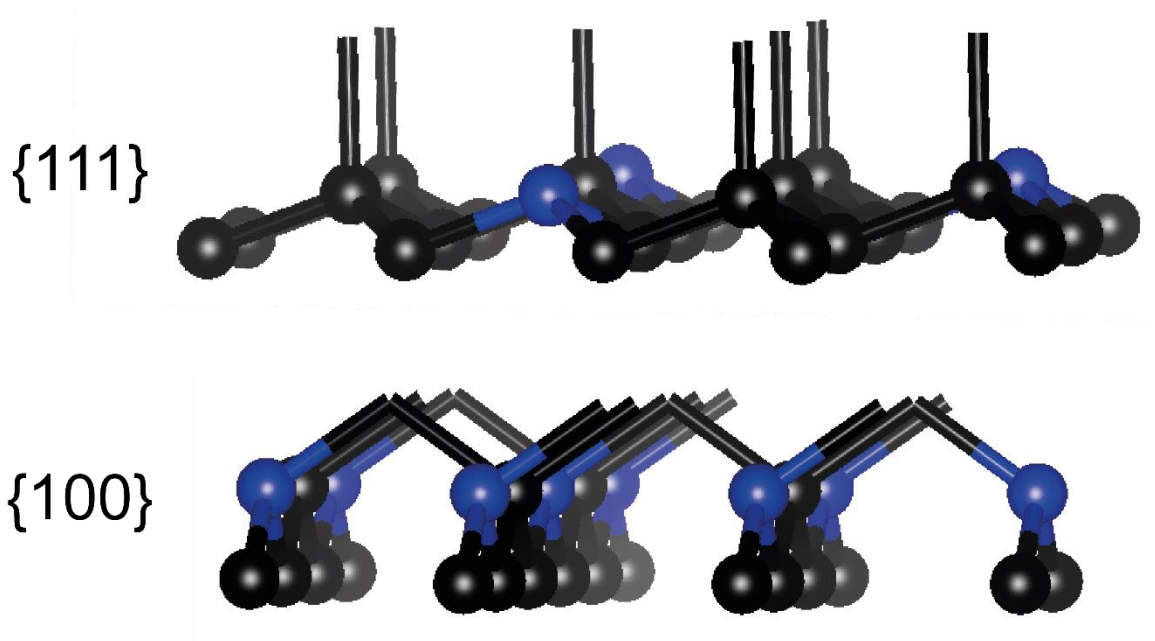

Figure S3. Schematic to show the dangling bonds present when boron (blue) is substituted for carbon (black) on the {111} and {100} growth faces of diamond. Image generated using Avogadro (version 1.2.0).[2]

ESI 4: EDS data of HPHT BDD particles

The EDS spectra shown in Fig. S4 clearly shows a very strong peak for carbon and a small peak for boron, as is expected for BDD. Signals for Fe, Ni, Co, and Al (potential contaminants) are not present. This is also shown in the EDS maps, whereby carbon and boron signals strongly correlate with BDD particle location, and Fe, Ni, Co, and Al signals are negligible.

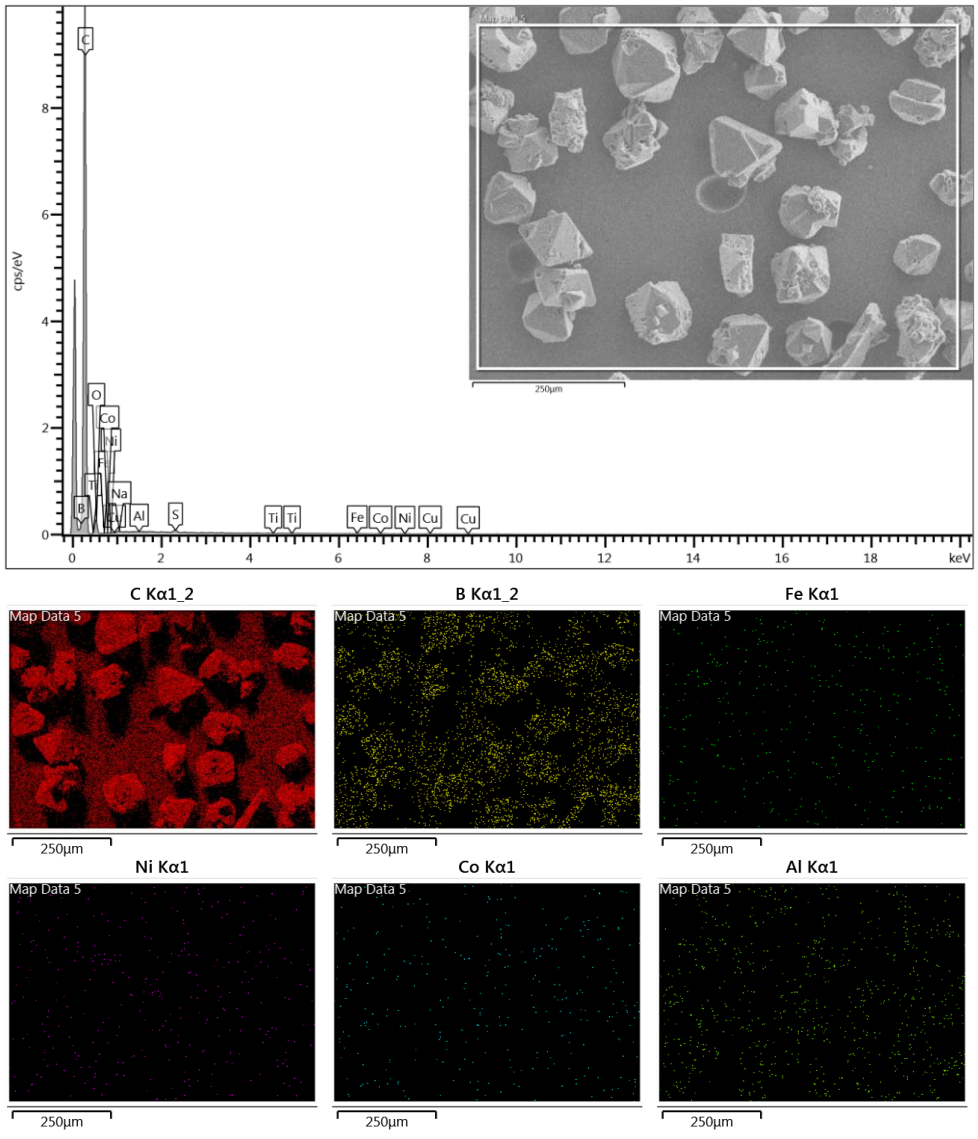

Figure S4. (a) EDS spectrum of HPHT BDD particles grown using 4.8 wt% AlB_2, with the EDS measurement area outlined in white in inset FE-SEM image. b) Elemental EDS maps of area shown in (a) for C, B, Fe, Ni, Co and Al.

ESI 5: Raman spectra of HPHT BDD particles

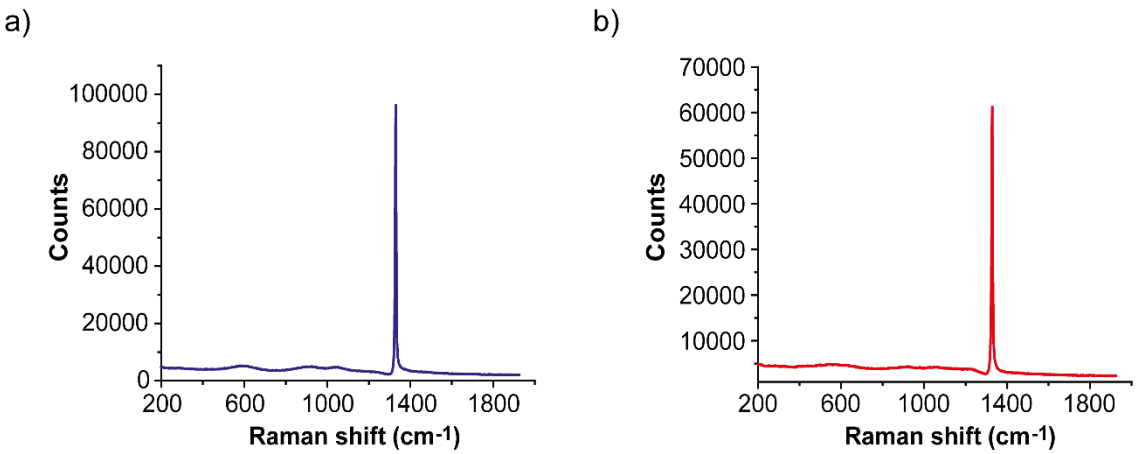

Figure S5. Typical Raman spectra recorded on an individual HPHT BDD particle grown using (a) 3.6% $AlBr_2$ and (b) 4.8% AlB_2. BDD peaks are observed at 550 cm^{-1} and 1200 cm^{-1}, along with an asymmetry due to a Fano resonance and red shift in the intrinsic diamond peak at 1330.8 cm^{-1} (3.6% AlB_2) and at 1329.2 cm^{-1} (4.8% AlB_2).

ESI 6: Compact HPHT BDD electrode resistance calculations

Four-point probe measurements of sheet resistance, R_s, were recorded to calculate the resistivity, ρ, of two HPHT BDD compact electrodes, one grown using 3.6 wt% AlB_2 and the other 4.8 wt% AlB_2. Four measurements were taken per compact, two in the forward direction and two in the reverse direction. ρ was calculated for each measurement using equation S1:

$$\rho = R_s t f_1 \qquad \text{(S1)}$$

where t is the compact thickness and f_1 is a finite thickness correction factor, given by table S1, where s is the spacing between probes.[3,4] The average of these four ρ values were taken to give 959 ± 96 mΩ cm and 646 ± 129 mΩ cm for 3.6 wt% AlB_2 and 4.8 wt% AlB_2, respectively. The resistance of the compacts, R, when operated as an electrode, was calculated using the equation for the resistance of a truncated cone (equation S2):

$$R = \frac{\rho L}{ab} \qquad \text{(S2)}$$

where, L is the length of the cone, and a and b are dimensions depicted in Fig. S12. In this case, a is the radius of the exposed top surface of the compact electrode (a = 0.5 mm), b is the radius of the bottom surface of the compact electrode and L is the thickness of the compact. Again, four values were calculated for each compact and the average taken to give 0.500 ± 0.06 Ω and 0.300 ± 0.03 Ω for the two compacts, 3.6 wt% AlB_2 and 4.8 wt% AlB_2, respectively.

t/s	f_1
2.50	0.520
2.55	0.515
2.60	0.510
2.65	0.495
2.70	0.480
2.75	0.475
2.80	0.470

Table S1. Finite thickness correction factor values.

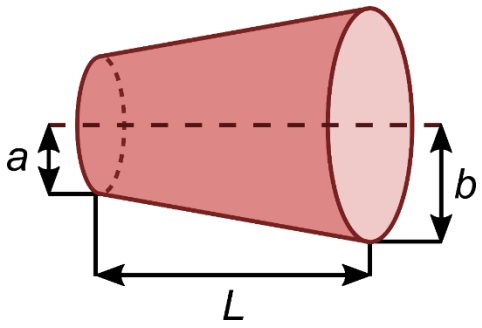

Figure S6. Schematic to show the key dimensions used to calculate the resistance of a truncated cone from resistivity measurements.

ESI 7: $Ru(NH_3)_6^{3+}$ response for CVD grown BDD

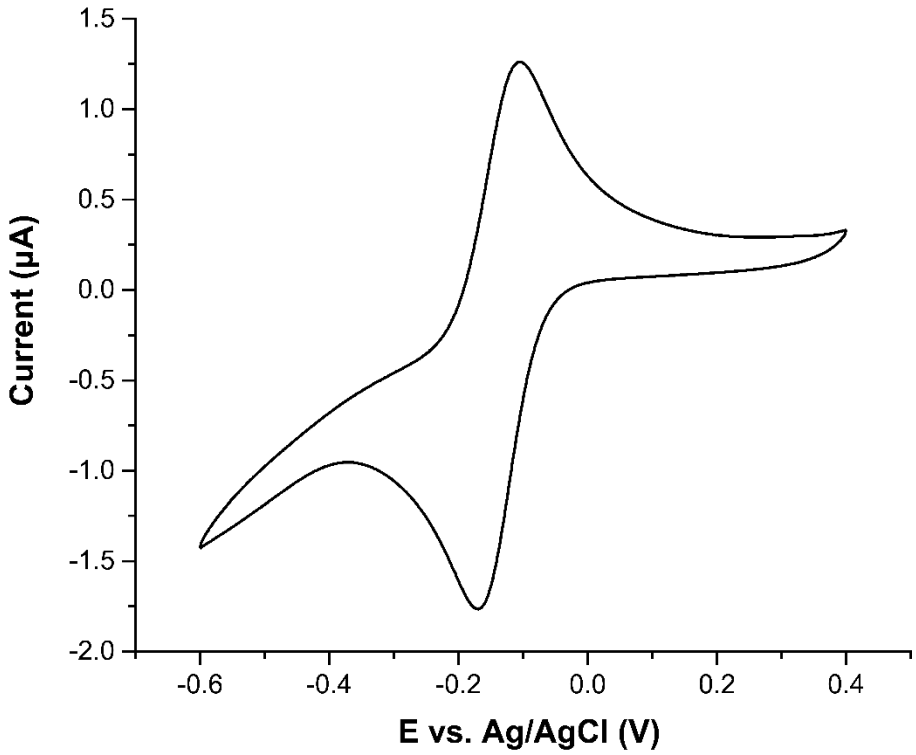

Figure S7. CV recorded in 0.1 M KNO_3 and 1 mM $Ru(NH_3)_6^{3+/2+}$ at a scan rate of 0.1 V s^{-1} to show the electrode response of CVD grown BDD, using a droplet electrochemical cell set-up as described in ESI 1. A peak to peak separation, ΔE_p, of 62 mV is observed.

ESI 8: Estimation of k_0 for high quality CVD grown BDD

DigiElch Electrochemical Simulation software was used to estimate the electron transfer rate constant, k_0, based on the peak to peak separation of *ca.* 0.6 V in Fig. 5b. The conditions of these SECCM experiments differ from conventional macroscopic experiments due to an enhanced mass transport originating from radial diffusion in the tip orifice.[5] However, because a fast scan rate was used in the reported experiments to minimise the contact time of the SECCM meniscus on the surface and solution wetting during each measurement, mass transport will predominantly be transient (planar diffusion) as evident from the CV response in Figure 5b in the main text. It should be noted that mass transport is by migration as well as diffusion, as the concentration of $Ru(NH_3)_6^{3+}$ and supporting electrolyte (10 mM KNO_3) was similar to prevent crystallization and blocking at the tip orifice. Thus the DigiElch calculations (planar diffusion) are approximate, but can be used to estimate the intrinisic rate constant, k_0 from the SECCM experiment (diameter of the working electrode d = 2.5 ± 0.2 µm , scan rate v = 10 V s^{-1}, and an uncompensated resistance of 15 MΩ from the nanopipette tip) giving a k_0 of 5 × 10^{-3} cm s^{-1}. This is slightly lower than earlier reported calculations for BDD[6] but reasonable given the approximations employed.

ESI 9: HPHT BDD compact coating by electropolymerisation of poly(oxyphenylene)

In order to investigate material porosity, the polished surface of a HPHT BDD compact was coated with a thin, uniform, pinhole free, insulating film of poly(oxyphenylene). This was achieved by the electropolymerisation of a freshly made solution containing 60 mM phenol, 90 mM 2-allyphenol, and 160 mM 2-n-butoxyethanol in water/methanol (1:1 by volume).[7] The pH of the monomer solution was adjusted by the addition of ammonium hydroxide, dropwise, until a pH of 9.2 was reached. A voltage of +2.5 V against a silver wire quasi-reference electrode was applied for 20 minutes. After deposition, the surface was rinsed in 1:1 water/methanol, and the copolymer film heat cured for 30 minutes at 150 °C. To remove the polymer coating, the HPHT BDD compact surface was gently polished using alumina micropolish (0.05 µm, Buehler) with a cotton bud, before rinsing with distilled water (Fig. S7).

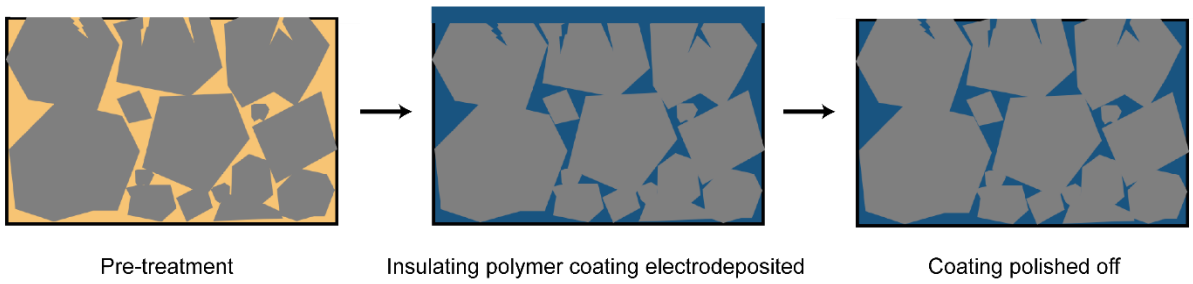

Figure S8. Cross sectional schematic to show the process of void (pore) filling a HPHT BDD compact by electrodeposition of a poly(oxyphenylene) film. The orange color represents the voids and the blue represents the insulating polymer. During polishing the top surface of the compact is revealed.

Prior to coating with poly(oxyphenylene), the CV for 1 mM $Ru(NH_3)_6^{3+}$ is shown in Fig. S9 (black line). When the insulating coating was applied, no electrochemical response is observed due to blocking of all accessible electron transfer sites (orange line). After gentle polishing of the top surface, the CV (pink line) is now clearly defined, smaller in current and significantly reduced in capacitive contributions. This is likely due to the coating filling the sub-surface

pores and thus limiting the exposed BDD area to only the top surface of the compact. A peak to peak separation in 1 mM $Ru(NH_3)_6^{3+}$ of 0.105 V was determined.

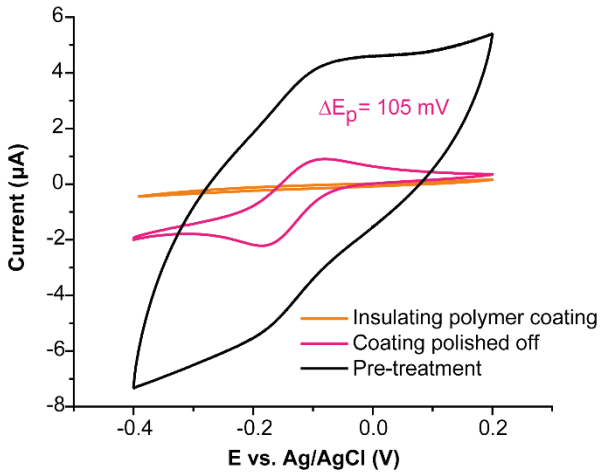

Figure S9. CVs recorded in 1 mM $Ru(NH_3)_6^{3+/2+}$ and 0.1 M KNO_3 at 0.1 V s^{-1} of a HPHT BDD compact grown using 4.8% AlB_2 before and after coating with poly(oxyphenylene), and after polishing of the coating.

ESI 10: MATLAB script for data reading

A script was written (in .mat format) to read the SECCM data corresponding to Fig. 6b (main text) using MATLAB (MathWorks). The data file "Data.mat" and the data reading script "DataReadingScript.m" for Fig. 6b are both provided and should be loaded into the MATLAB workspace. Running the script generates an interactive figure (Fig. S12) with a map on the left hand side showing the onset potentials, pixel by pixel, and a CV on the right hand side that corresponds to the selected pixel. Clicking on a desired pixel provides the corresponding CV. The script was developed and tested in a Matlab R2018a environment and provides flexible data visualisation.

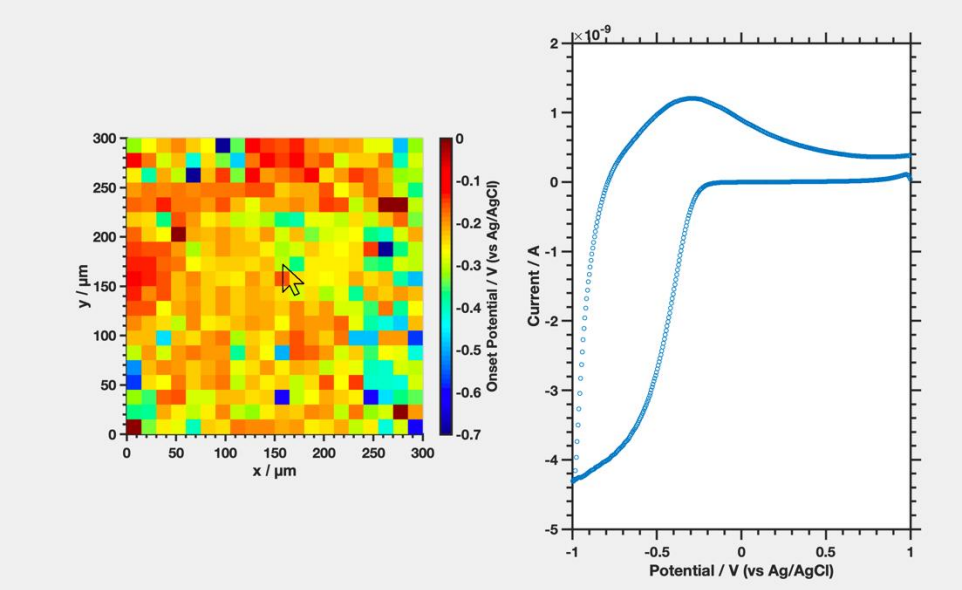

Figure S10. Screenshot of the MATLAB script window for reading SECCM data. The map on the left shows the spatial distribution of onset potentials. The left-button mouse click on the map generates an individual CV on the right part of the window recorded on the chosen pixel. Each CV follows from the onward cathodic sweep from +1 V to -1 V and continues to the anodic sweep back to +1 V.

ESI 11: FE-SEM images of SECCM scan area

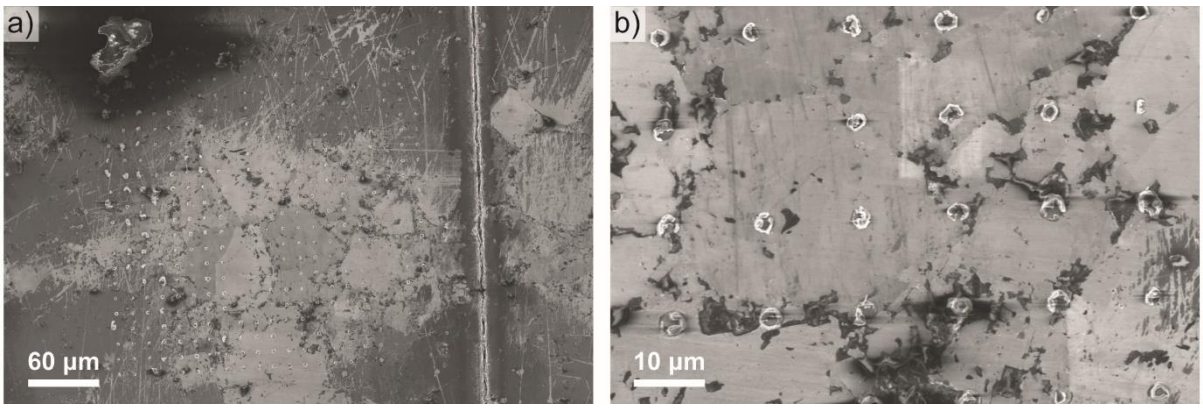

Figure S11. FE-SEM secondary electron images of the SECCM scanned region shown in Fig. 6 of the HPHT BDD compact, grown using 4.8 wt% AlB_2 at (a) 200× and (b) 1200× magnification. Meniscus residues are clearly visible in both images indicating the spatial locations of the capillary. The large salt crystal visible in the upper left corner of (a) is residual KNO_3 from deliberately crashing the nanopipette tip into the electrode surface at the end of the SECCM scan, a strategy adopted to simplify detection of the scanned area in SEM.

ESI 12: SECCM capacitance time delay

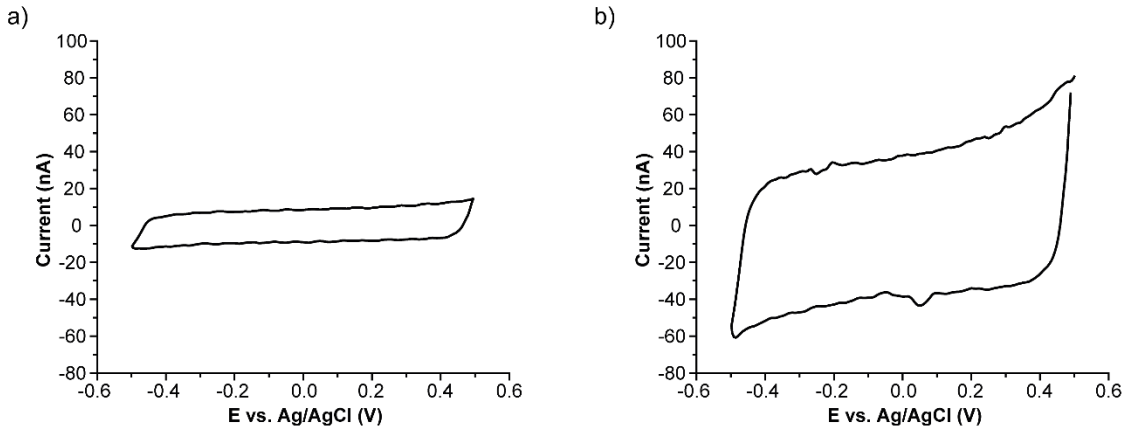

Figure S12. Typical capacitance CVs recorded in 0.01 M KNO_3 at 10 V s^{-1} during an SECCM scan of a HPHT BDD compact, grown using 4.8 wt% AlB_2 after (a) immediate contact of droplet to electrode surface and (b) after a 1 second delay. The values of capacitance estimated from capacitance CVs recorded at each pixel over the whole SECCM scan area (*n*=400) are (a) 12 ± 3.6 μF cm^{-2} and (b) 56 ± 17 μF cm^{-2}.

References

[1] J.Q. Zhang, H.A. Ma, Y.P. Jiang, Z.Z. Liang, Y. Tian, X. Jia, Effects of the additive boron on diamond crystals synthesized in the system of Fe-based alloy and carbon at HPHT, Diam. Relat. Mater. 16 (2007) 283–287. doi:10.1016/j.diamond.2006.06.005.

[2] M.D. Hanwell, D.E. Curtis, D.C. Lonie, T. Vandermeerschd, E. Zurek, G.R. Hutchison, Avogadro: An advanced semantic chemical editor, visualization, and analysis platform, J. Cheminform. (2012). doi:10.1186/1758-2946-4-17.

[3] Finite-Size Corrections for 4-Point Probe Measurements, (n.d.).

[4] F.M. Smits, Measurement of Sheet Resistivities with the Four-Point Probe, Bell Syst. Tech. J. 37 (1958) 711–718. doi:10.1002/j.1538-7305.1958.tb03883.x.

[5] D.A. Walsh, J.L. Fernández, J. Mauzeroll, A.J. Bard, Scanning electrochemical microscopy. 55. Fabrication and characterization of micropipet probes, Anal. Chem. 77 (2005) 5182–5188. doi:10.1021/ac0505122.

[6] L.A. Hutton, J.G. Iacobini, E. Bitziou, R.B. Channon, M.E. Newton, J. V Macpherson, Examination of the Factors Affecting the Electrochemical Performance of Oxygen-Terminated Polycrystalline Boron-Doped Diamond Electrodes, Anal. Chem. 85 (2013) 7230–7240. doi:10.1021/ac4010421.

[7] D.P. Burt, N.R. Wilson, J.M.R.R. Weaver, P.S. Dobson, J. V. Macpherson, Nanowire probes for high resolution combined scanning electrochemical microscopy - Atomic force microscopy, Nano Lett. 5 (2005) 639–643. doi:10.1021/nl050018d.